Chapter 5

Estimating the Cd^{2+} adsorption efficiency on nanotubular halloysites in weathered pegmatites using optimized artificial neural networks: Insights into predictive model development

Mark A. Engle[a], Hoang-Bac Bui[b,c], and Hoa Anh Nguyen[d]
[a]*Department of Earth, Environmental and Resource Sciences, The University of Texas at El Paso, El Paso, TX, United States,* [b]*Department of Exploration Geology, Faculty of Geosciences and Geoengineering, Hanoi University of Mining and Geology, Hanoi, Vietnam,* [c]*HiTech-CEAE Research Team, Hanoi University of Mining and Geology, Hanoi, Vietnam,* [d]*Faculty of Basic Sciences, Hanoi University of Mining and Geology, Hanoi, Vietnam*

1 Introduction

Over the last few decades, heavy metal pollution has become a widespread environmental concern due to the surge in industrialization across the world. Some of the most toxic heavy metals include copper, cadmium, nickel, chromium, arsenic, mercury, lead, and others, which pose a threat to human health and aquatic ecosystems [1]. These metals have a persistent presence in the environment as they are non-biodegradable and do not break down over time. Developing countries are particularly susceptible to heavy metal pollution from various industrial activities, such as mining, smelting, and tanning, which can release these harmful substances into the environment [2–4]. Consequently, exposure to heavy metals through drinking water and the food chain is a concern for human health.

Many researchers have studied the issue of heavy metal absorption or removal in water, wastewater, and soils, with a focus on water as it makes

Applications of Artificial Intelligence in Mining and Geotechnical Engineering
https://doi.org/10.1016/B978-0-443-18764-3.00020-5

up only 2.5% of the earth's freshwater and is crucial for human daily life [5–7]. To absorb heavy metals from water, several biochar systems and materials have been proposed and tested, including graphene oxide and its composites, polyacrylamide oxide hydrogel grafted sodium alginate, thiosemicarbazide nanocomposite, electrospun nanofibrous membranes, and thiol-functionalized cellulose nanofiber membranes. These materials have shown promising results in removing heavy metals such as Cd^{2+}, Cu^{2+}, Ni^{2+}, Pb^{2+}, and Cu^{2+}. More information on these materials can be found in the literature [8–10].

Of those heavy metals, Cd^{2+} was recommended as one of the most dangerous heavy metals and it has been studied, evaluated, and removed by many researchers with different materials. Indeed, a study has been conducted to evaluate the effectiveness of a hydrogel made of polyacrylamide/carboxymethyl guar gum (PAM/CMG) containing meta-benziporphodimethene (meta-BPDM) ligand for the selective removal of Zn^{2+}, Cd^{2+}, and Hg^{2+} ions from water [11]. Batch adsorption experiments were conducted to investigate the effects of pH, initial metal ion concentration, and contact time on the removal of metal ions. The maximum removal of metal ions was observed at pH 6.5, and the sorption equilibrium was achieved in 8 h, 12 h, and 6 h contact time for Zn^{2+}, Cd^{2+}, and Hg^{2+} ions, respectively. The hydrogel exhibited a higher adsorption capacity and selectivity compared to other adsorbents studied. In a separate study, immobilized *Turbinaria ornata* biomasses were used for the biosorption of Cd^{2+} ions from aqueous solutions, with immobilized cells exhibiting a higher maximum removal efficiency compared to free cells [12]. The biosorption data were analyzed using Langmuir, Freundlich, and Temkin isotherm models. The immobilized algal biomass showed a maximum biosorption capacity of $29.6\,mg\,g^{-1}$ compared to $23.9\,mg\,g^{-1}$ for free cells. A covalent organic framework (COF) made of a nitrogen-oxygen-rich porphyrin-based material was also prepared, which showed a high adsorption capacity for Cd^{2+} [13]. The resulting optical signal changes enabled ratiometric detection of Cd^{2+}. The porphyrin COF-based carbon fiber (CF) membrane was demonstrated to effectively remove and enrich Cd^{2+} from soil and water samples. Finally, the simultaneous removal of Pb^{2+}, Cd^{2+}, and Hg^{2+} from aqueous solutions was investigated using porous geopolymers made from volcanic ash [14].

Researchers have used advanced techniques to measure the heavy metal absorption ability of various materials with different methods. Singh et al. [15] applied radial basis function neural networks (RBFNs) and multilayer perceptron neural networks (MLPNs), support vector machine, and gene expression programming to predict the absorption of chlorophenol. The MLPN and RBFN models performed better than the other models. Fawzy et al. [16] also developed an artificial neural network (ANN) model to estimate the removal efficiency of Cd^{2+}. Their study showed a high fit with an R^2 of 0.923. Dolatabadi et al. [17] used an artificial neural network and adaptive neuro-fuzzy inference system model to predict the removal of heavy metals from an aqueous solution using sawdust. The models were promising simulation techniques

for heavy metal removal processes. Fan et al. [18] conducted a review of machine learning algorithms like ANN, genetic algorithm (GA), and particle swarm optimization (PSO) in terms of modeling heavy metal removal processes. They concluded that GA-ANN and PSO-ANN models can successfully model the removal of heavy metals with accurate results. Lu et al. [19] built an artificial neural network and support vector machine models to simulate heavy metal concentrations with a promising result. Rahnama et al. [20] developed radial basis function and adaptive neuro-fuzzy inference system-based models to predict the sodium absorption rate of an aqueous solution. The radial basis function model was found to be an appropriate model for sodium absorption prediction. El Hanandeh et al. [21] used artificial neural networks and multi-input multi-output models to predict the heavy metal absorption capacity onto biochar with a promising result ($R^2 = 0.99$). Rodríguez-Romero et al. [22] used pyrolysis and $ZnCl_2$ activation to remove As_{2+} from water and modeled the absorption kinetics and isotherms results using an artificial neural network model. Similar studies can be found in the literature [23–31].

Many researchers have used various materials and artificial intelligence techniques to study heavy metal removal and predict the absorption efficiency of different materials. In this study, the authors focused on the use of nanotube-type halloysite from weathered pegmatites for absorbing heavy metals. Cd^{2+} was selected as a case study due to its negative health effects as warned by the World Health Organization. In this chapter, the authors proposed and compared three novel hybrid models based on the ANN model and metaheuristic optimization algorithms, including PSO, Differential Evolution (DE), and Slime Mold Algorithm (SMA), called PSO-ANN, DE-ANN, and SMA-ANN models. The detail of the methodology and dataset as well as obtained results are presented and discussed in the following sections.

2 Materials description

The halloysite sample was obtained from the Lang Dong, Thach Khoan, and Phu Tho kaolin mines after the screening process. The samples were mixed and filtered evenly using the wet sieving method with a 32 μm mesh size. The material under the sieve was dried and filtered, then dried again at 60°C. The dried sample was used for testing and analysis in the subsequent steps.

In this study, the ability of halloysite in adsorbing Cd^{2+} was investigated by adding a predetermined amount of halloysite to a 50 mL container of a simulated waste solution containing Cd^{2+} ions. The simulated waste solution was prepared by dissolving $Cd(NO_3)_2.4H_2O$ salts in water at different concentrations in the laboratory, and the pH of the solution was adjusted using 0.01 M HCl or 0.01 M NaOH solution. The adsorption process was found to be influenced by various factors, including contact time (CT), pH, amount of adsorbent (AW), and initial concentration of Cd^{2+} in the solution ($Cd_{initial}$), as shown in Table 1.

TABLE 1 The adsorption process of halloysite samples.

$Cd_{initial}$	pH	AW	CT	Cd_{output}
45	6.3	0.6	45	24.334
45	6.3	0.6	55	22.638
45	6.3	0.6	70	22.952
45	6.3	0.6	90	22.347
80	6.3	0.4	45	60.89
80	6.3	0.4	55	60.143
80	6.3	0.4	70	60.127
80	6.3	0.4	90	51.875
70	6.3	0.6	45	40.617
70	6.3	0.6	55	38.138
70	6.3	0.6	70	36.347
70	6.3	0.6	90	34.114
45	6.8	0.6	45	22.087
45	6.8	0.6	55	20.756
45	6.8	0.6	70	22.239
45	6.8	0.6	90	19.299
80	6.8	0.4	45	60.619
80	6.8	0.4	55	59.261
80	6.8	0.4	70	58.344
80	6.8	0.4	90	56.645
70	6.8	0.6	45	41.667
70	6.8	0.6	55	41.171
70	6.8	0.6	70	40.999
70	6.8	0.6	90	39.256
46	6.2	0.5	10	46
46	6.2	0.5	20	22.93
46	6.2	0.5	30	21.154
46	6.2	0.5	40	20.68
46	6.2	0.5	50	18.076

TABLE 1 The adsorption process of halloysite samples—cont'd

$Cd_{initial}$	pH	AW	CT	Cd_{output}
46	6.2	0.5	60	17.852
46	6.2	0.5	70	17.746
46	6.2	0.5	80	17.089
46	6.2	0.5	100	17.076
46	6.2	0.5	120	17.036
46	2.95	0.5	50	25.263
46	4	0.5	50	24.113
46	4.95	0.5	50	21.036
46	5.5	0.5	50	19.733
46	6	0.5	50	18.905
46	6.5	0.5	50	18.55
46	7	0.5	50	17.574
46	8	0.5	50	16.527
46	8.8	0.5	50	10.263
46	6.5	0.3	50	23.521
46	6.5	0.5	50	18.55
46	6.5	0.7	50	17.905
46	6.5	0.8	50	17.574
46	6.5	0.9	50	16.431
46	6.5	1	50	14.406
20	6.5	0.8	50	2.132
30	6.5	0.8	50	4.108
40	6.5	0.8	50	10.5
50	6.5	0.8	50	17.603
60	6.5	0.8	50	22.101
70	6.5	0.8	50	32.636
80	6.5	0.8	50	37.963

To study the ability of halloysite to adsorb Cd^{2+}, a sample of halloysite minerals was collected from the Lang Dong, Thach Khoan, and Phu Tho kaolin mines and then subjected to wet sieving using a 32 μm mesh size. The resulting sample was dried at 60°C and used for subsequent testing and analysis. The experiment involved adding a certain amount of the halloysite material to a 50 mL container containing a simulated waste solution with Cd^{2+} ions at varying concentrations. The pH level of the solution was adjusted using 0.01 M HCl or 0.01 M NaOH, and the adsorption process was studied based on several factors, including contact time, pH, amount of adsorbent, and initial concentration of Cd^{2+} in the solution. The mixture was stirred with an 800 RPM stirrer for varying adsorption times, pH levels, and amounts of halloysite powder. After adsorption, the solid matter was filtered out, and the remaining Cd^{2+} ions in the solution were quantified using ICP-MS. Overall, the results of the study provide insight into the potential use of halloysite as an effective adsorbent for Cd^{2+} ions in waste solutions. Fig. 1 shows the halloysite minerals and the progress to analyze halloysite for environmental purposes.

3 Artificial neural network

An ANN is made up of interconnected units, which can be single or multiple layers. The input data is fed into input neurons (synapses) where it is assigned a weight by the software. This weighted sum is then processed by an activation function, and the output data is passed on to other neurons within the network [32]. The neurons are connected in such a way that the activation values can contribute to the final result or be used as input for a subsequent model. The connection weights are adjusted during the training to improve the accuracy of the model. The network is trained by exposing it to a series of training patterns and modifying the weights until the desired level of accuracy is achieved [33]. A visual representation of a simplified ANN is shown in Fig. 2.

In the current study, a multi-layer perceptron (MLP) network with backward propagation (BP) was selected because it is effective in modeling nonlinear multivariate systems [34]. The MLP network has an input layer that receives the input data and an output layer that produces the output vector. Additionally, it has hidden layers that do not receive direct input and do not contribute directly to the output. The input signals are transformed as they move in a forward direction toward the output layer. The activation function for neurons in an MLP network can be linear or non-linear, using functions such as logarithmic, linear, hyperbolic tangent, and sigmoidal, among others [35]. For this study, the hyperbolic tangent function was used in the analysis and adjustment of equations because it is the most commonly used function in an MLP configuration (as shown in Eq. (1)).

$$\tanh(x) = \frac{e^{x} - e^{-x}}{e^{x} + e^{-x}},$$

where e is Euler's number (approximately 2.71828), and x is the input value.

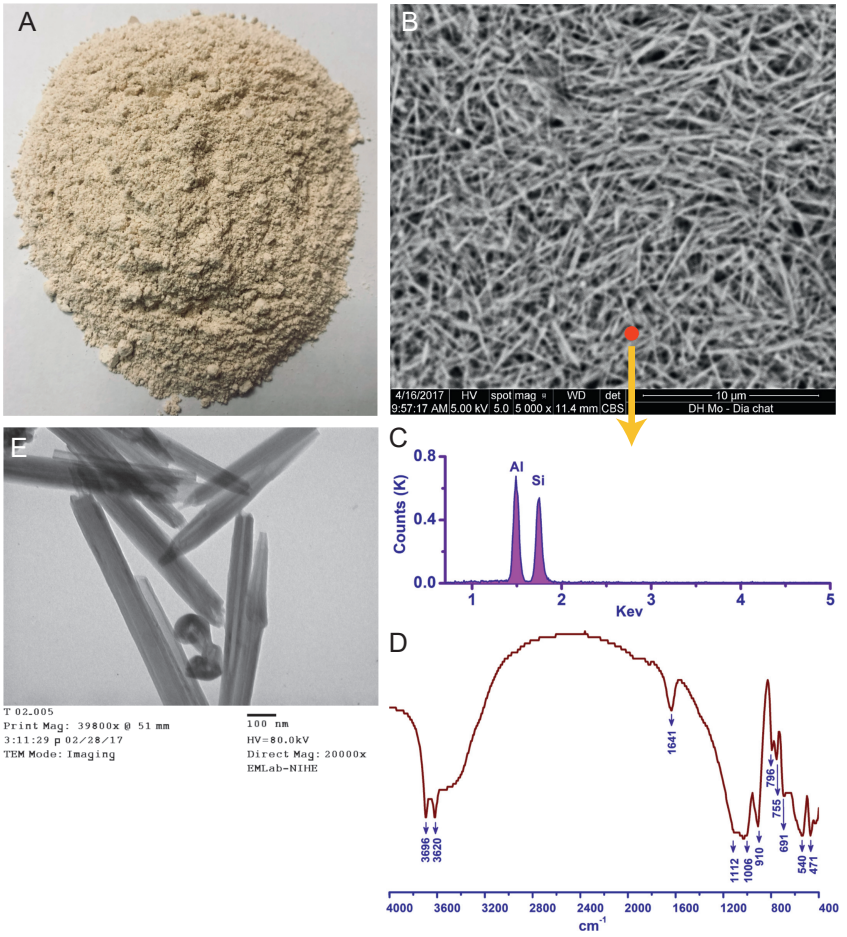

FIG. 1 Various aspects of halloysite minerals. (A) A sample of halloysite minerals, (B) an SEM image of the sample with rod-shaped halloysite minerals overlaid onto a matrix, (C) the identification of elements in the halloysite mineral through the EDS pattern, (D) the results of FT-IR analysis, and (E) a TEM image showing the tubular structure of halloysite minerals.

4 Optimization algorithms used

4.1 Slime mold algorithm

The SMA is an optimization algorithm inspired by the behavior of the *Physarum polycephalum*, a type of slime mold [36]. It models the behavior of the slime mold as it moves toward food sources in its environment.

In the SMA, the optimization problem is represented as a graph, with nodes representing potential solutions and edges representing the feasibility between solutions. The algorithm begins by initializing the position of a virtual "slime mold" on the graph. The slime mold then moves from node to node, based on the

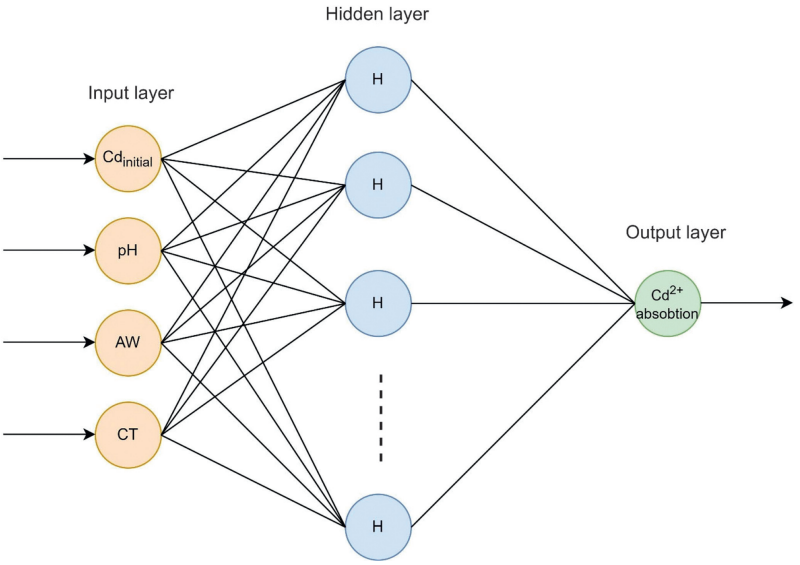

FIG. 2 Structure of an ANN model for predicting Cd^{2+} absorption.

intensity of the "smell" or attraction at each node, until it reaches the node with the highest smell intensity [37].

At each iteration, the slime mold's position is updated based on a combination of its current position and the positions of other "particles" in the optimization search space. The algorithm also includes a random exploration component, allowing the slime mold to move away from the current optimal solution and search for better solutions.

The algorithm continues until a stopping criterion is met, such as reaching a maximum number of iterations or finding a solution with a sufficient level of fitness. The final solution is the node with the highest smell intensity, which represents the best solution found by the algorithm.

4.2 Particle swarm optimization

The PSO algorithm is a population-based and intelligent optimization method that simulates the behavior of complex adaptive systems [38]. It consists of a set of particles that move in a multidimensional search space and adapt their movement based on their experience and the experience of other particles in the swarm. The basic mechanism of the PSO algorithm is presented through the six following steps:

(Step 1) Initialization: The positions and velocities of the particles in the swarm are initialized randomly within a defined search space.

(Step 2) Fitness calculation: The fitness of each particle is evaluated using a predefined objective function.

(Step 3) Velocity and position update: Based on the current fitness values and the historical best positions of the particles, the velocities and positions of the particles are updated.

(Step 4) Global best update: The best position among all particles in the swarm is updated and used to guide the movement of other particles.

(Step 5) Terminal condition check: The algorithm terminates when a predefined stopping criterion is met, such as a maximum number of iterations or a desired level of accuracy.

(Step 6) Output: The particle with the best fitness value is returned as the solution to the optimization problem.

The PSO algorithm repeatedly updates the positions and velocities of the particles in the swarm, seeking the global optimal solution to the optimization problem. Further detail of the PSO algorithm can be found in the literature [39–42].

4.3 Differential evolution

The DE algorithm is a stochastic, population-based optimization method. It works by iteratively adjusting the values of candidate solutions in a population toward the best solution [43,44]. The algorithm is operated through the following five steps:

(Step 1) Initialization: A population of candidate solutions is randomly generated and each solution is represented by a vector of real numbers.

(Step 2) Mutation: A new candidate solution is generated by combining the values of three randomly selected solutions in the population. The new candidate is created by adding a weighted difference between two randomly selected solutions to a third solution.

(Step 3) Crossover: A random number is generated for each component of the new candidate solution. If the number is below a predefined probability, the value of the component is replaced with the corresponding component from the new candidate solution.

(Step 4) Selection: The fitness of the new candidate solution is evaluated and compared with the fitness of the original solution. If the new candidate has better fitness, it is accepted as the new solution.

(Step 5) Iteration: Steps 2–4 are repeated until a stopping criterion is met, such as a maximum number of iterations or a satisfactory level of solution quality.

The DE algorithm is known for its ease of implementation, its ability to handle multi-modal and nonlinear optimization problems, and its robustness in the presence of noise [45,46].

5 Framework of optimized artificial neural networks

In this book chapter, the ANN model is used as the primary model for predicting Cd^{2+} absorption by the halloysite. Normally, the ANN model is often trained by back-propagation algorithm. However, it might be stuck in the local optimal and lead to low convergence and accuracy [47–49].

To overcome this disadvantage, metaheuristic algorithms are considered a potential approach that can provide more optimal solutions with optimized weights of the ANN model. In other words, the weights of the ANN model can be optimized by metaheuristic algorithms by their global optimization mechanisms. Herein, the PSO, SMA, and DE algorithms were used to deal with this problem.

In this way, both the PSO, SMA, and DE algorithms generated a variety of solutions based on the initial populations, and each population acted as a solution with a set of weights that will be optimized to minimize the loss of the fitness function (i.e., MSE). The optimized weights were then transferred to the ANN model and its performance was calculated and evaluated through the stopping conditions, such as the number of iterations and error. Finally, the best weights with the lowest MSE will be selected as the best parameters of the ANN model, and they will be applied to predicting Cd^{2+}, named PSO-ANN, SMA-ANN, and DE-ANN models. The framework of these models is presented in Fig. 3.

6 Estimation of Cd^{2+} adsorption efficiency of halloysite

For estimation of the Cd^{2+} adsorption efficiency of halloysite, the dataset containing pH, CT, AW, and $Cd_{initial}$ parameters were used to explain the relationship between these input parameters and Cd^{2+} adsorption efficiency of halloysite. The dataset was divided into two parts including the training dataset (containing 70% of the whole dataset) and the testing dataset (containing the remaining 30% of the dataset). Whereas the training dataset was applied to develop the PSO-ANN, SMA-ANN, and DE-ANN models, the testing dataset was applied to evaluate the performance of the developed models. It should be noted that this task was randomly separated.

Before training the ANN model, a network topology with a single hidden layer containing ten hidden nodes were designed. The "ReLU" activation function was used to transfer data between the layers, and the dropout technique with a value of 0.2 was applied to prevent the overfitting of the model. The metaheuristic algorithms were set up based on their parameters, with various populations (20, 100, 150, 200, 250, 300) computed for 500 iterations. The MSE function was used as the loss function during the training of the ANN model by the PSO, SMA, and DE algorithms with various parameters, as mentioned before. The 5-fold cross-validation technique was also applied to evaluate the models during the training process for more objectives. Their performance is shown in Fig. 4.

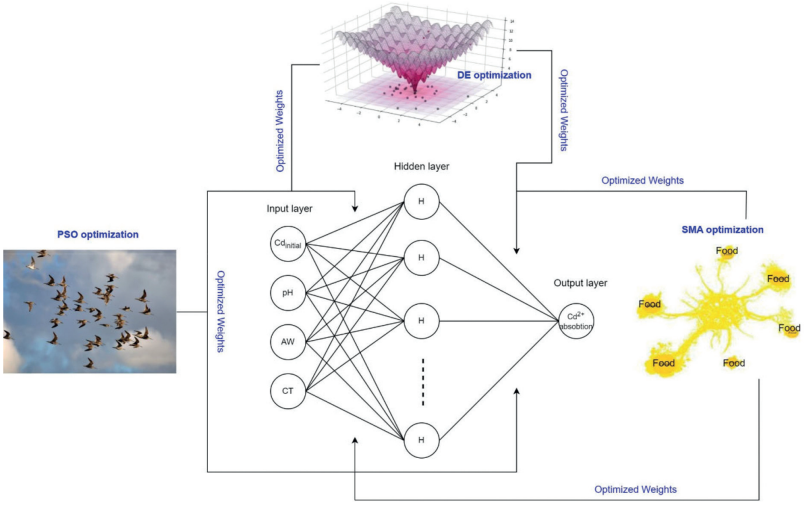

FIG. 3 The framework of the PSO-ANN, SMA-ANN, and DE-ANN models for predicting Cd^{2+} absorption by halloysite.

Based on the errors of the models presented in Fig. 4, we can determine the optimal population size for each model as follows: The DE-ANN model requires 250 populations, the PSO-ANN model requires 200 populations, and the SMA-ANN model requires 300 populations. However, to fully evaluate the performance of the models, we should consider the testing loss to determine whether they are overfitting or not. Additionally, in Fig. 5, we compared the training and testing convergences. The detail of the results is discussed in the following section.

Once the best models were defined, they were used to predict the Cd^{2+} absorption efficiency of halloysite on the testing dataset. It should be noted that the testing dataset has not been used during the training of the DE-ANN, PSO-ANN, and SMA-ANN models, and it can be evaluated as an unseen dataset. The predictions are shown in Tables 2 and 3. Then, they were used to compute the performance metrics of the models based on the Root Mean Squared Error (RMSE), Mean Absolute Error (MAE), and *R*-squared (R^2) functions, as shown in Table 4. Finally, the testing results are illustrated in Fig. 6.

7 Discussion

Tables 2–4 show the predicted values of Cd^{2+} absorption efficiency by the developed models (i.e., DE-ANN, PSO-ANN, and SMA-ANN) on both the training and testing datasets, as well as the performance metrics of the models for estimating Cd^{2+} absorption by halloysite.

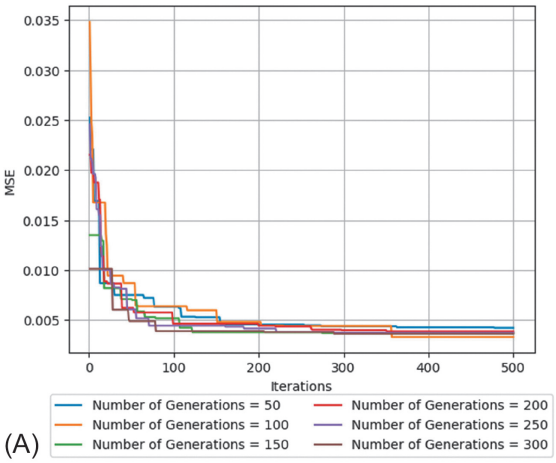

(A)

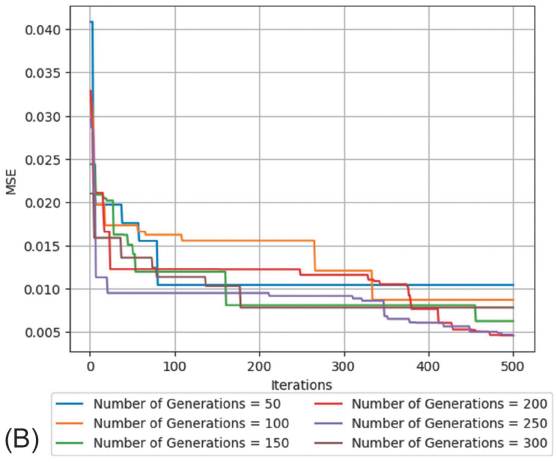

(B)

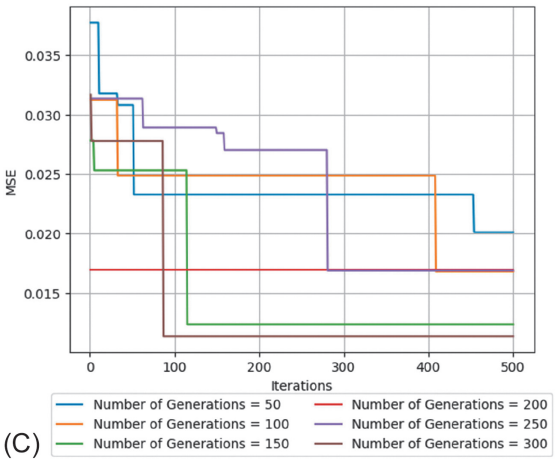

(C)

FIG. 4 Training performance of the models with various population sizes. (A) DE-ANN model. (B) PSO-ANN model. (C) SMA-ANN model.

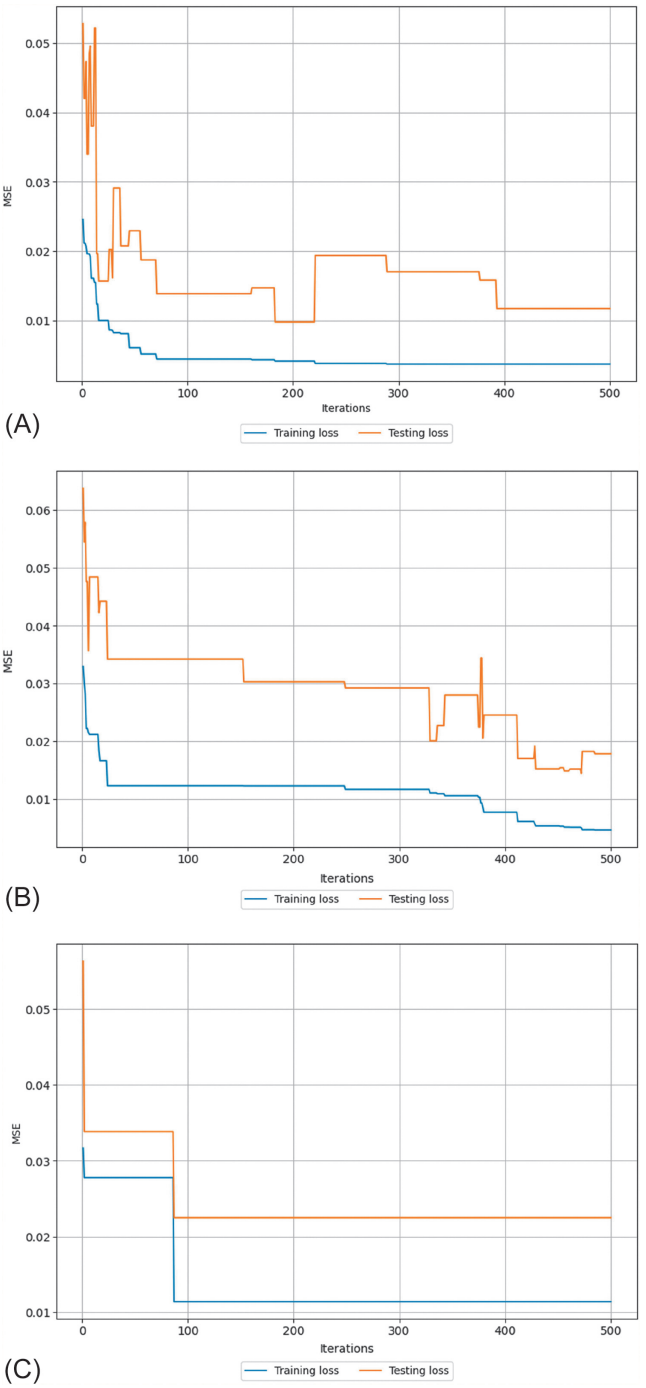

FIG. 5 Training and testing losses of the AI-based models in estimating Cd^{2+} absorption by halloysite. (A) Convergence of the DE-MLP model. (B) Convergence of the PSO-MLP model. (C) Convergence of the SMA-MLP model.

TABLE 2 Resulting of the Cd^{2+} absorption efficiency prediction by the developed models on the training dataset.

Actual Cd^{2+} absorption efficiency	Predicted Cd^{2+} absorption efficiency by the DE-ANN model	Predicted Cd^{2+} absorption efficiency by the PSO-ANN model	Predicted Cd^{2+} absorption efficiency by the SMA-ANN model
39.256	38.604	39.640	39.149
17.036	21.671	16.882	29.528
10.5	13.355	9.552	18.864
17.852	20.289	20.471	24.074
24.334	18.294	16.838	19.143
22.239	17.831	15.642	19.427
18.905	20.967	21.061	23.812
17.603	16.975	14.806	20.739
17.746	20.201	20.164	24.699
36.347	39.996	41.294	38.790
22.347	17.932	15.699	20.895
22.93	24.193	21.732	21.666
23.521	27.842	27.713	31.164
16.431	13.641	10.522	20.282
20.756	17.950	16.012	18.862
18.55	20.353	20.366	22.932
60.127	54.844	52.804	52.074
18.55	20.353	20.366	22.932
17.905	17.270	14.578	19.589
19.733	21.911	21.773	24.710
60.619	55.389	53.304	50.606
56.645	54.277	51.755	52.267
10.263	20.113	17.397	21.166
4.108	10.068	6.733	17.130
41.171	40.801	41.101	36.867
17.574	20.203	19.688	22.072

TABLE 2 Resulting of the Cd^{2+} absorption efficiency prediction by the developed models on the training dataset—cont'd

Actual Cd^{2+} absorption efficiency	Predicted Cd^{2+} absorption efficiency by the DE-ANN model	Predicted Cd^{2+} absorption efficiency by the PSO-ANN model	Predicted Cd^{2+} absorption efficiency by the SMA-ANN model
17.076	20.972	18.459	26.622
25.263	26.400	25.635	32.307
51.875	54.331	51.962	52.748
40.999	39.871	40.590	37.854
34.114	38.732	40.125	40.063
41.667	41.410	41.439	36.202
38.138	40.923	41.852	37.816
32.636	30.984	33.971	27.480
18.076	20.650	20.781	23.458
17.089	20.289	19.861	25.333
19.299	17.820	15.162	20.400
21.154	22.973	21.412	22.253
24.113	24.934	24.002	28.951

TABLE 3 Resulting of the Cd^{2+} absorption efficiency prediction by the developed models on the testing dataset.

Actual Cd^{2+} absorption efficiency	Predicted Cd^{2+} absorption efficiency by the DE-ANN model	Predicted Cd^{2+} absorption efficiency by the PSO-ANN model	Predicted Cd^{2+} absorption efficiency by the SMA-ANN model
39.256	55.434	53.536	51.165
17.036	18.030	16.263	18.870
10.5	15.433	12.345	19.972
17.852	8.068	5.490	15.545
24.334	12.083	9.110	20.007

Continued

TABLE 3 Resulting of the Cd^{2+} absorption efficiency prediction by the developed models on the testing dataset—cont'd

Actual Cd^{2+} absorption efficiency	Predicted Cd^{2+} absorption efficiency by the DE-ANN model	Predicted Cd^{2+} absorption efficiency by the PSO-ANN model	Predicted Cd^{2+} absorption efficiency by the SMA-ANN model
22.239	55.205	53.250	51.537
18.905	54.795	52.552	51.559
17.603	22.992	22.575	25.994
17.746	40.818	44.262	35.525
36.347	18.092	16.196	20.047
22.347	19.907	18.386	21.423
22.93	55.158	53.011	50.996
23.521	41.531	42.183	37.159
16.431	18.213	16.578	19.489
20.756	22.293	23.233	22.747
18.55	25.448	22.371	21.089
60.127	21.791	21.095	22.850

TABLE 4 Performance metrics of the intelligence models for estimating Cd^{2+} absorption by halloysite.

	Training dataset			Testing dataset		
Model	*MAE*	*RMSE*	R^2	*MAE*	*RMSE*	R^2
DE-MLP	2.855	3.442	0.936	4.279	6.118	0.887
PSO-MLP	3.528	4.472	0.892	5.344	6.588	0.869
SMA-MLP	5.064	6.017	0.805	6.326	8.474	0.783

Looking at Table 2, we can see that the predicted Cd^{2+} absorption efficiency values by the DE-ANN, PSO-ANN, and SMA-ANN models on the training dataset are close to the actual values. However, some of the predicted values deviate from the actual values by a large margin, such as the second row where

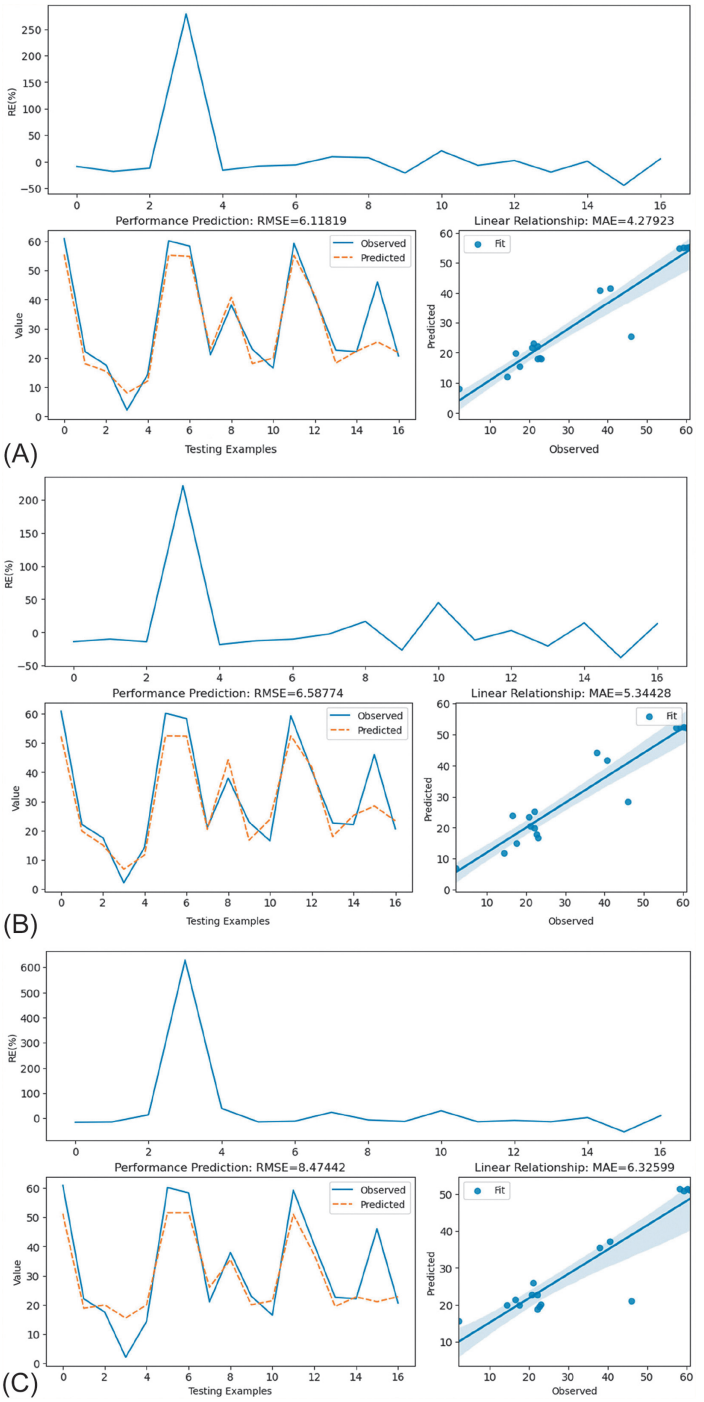

FIG. 6 The accuracy of the developed models for estimating Cd^{2+} absorption by halloysite. (A) DE-ANN model, (B) PSO-ANN model, and (C) SMA-ANN model.

the actual value is 17.036 while the predicted value by the PSO-ANN model is 16.882. Overall, the three models seem to perform reasonably well on the training dataset.

Whereas Table 2 shows the performance of the developed models on the training dataset, Table 3 shows the predicted values of Cd^{2+} absorption efficiency by the same models on the testing dataset. We can see that the predicted values deviate from the actual values by a larger margin compared to the training dataset, and this can also see in Fig. 6. For example, in the first row, the actual value is 39.256 while the predicted value by the DE-ANN model is 55.434. The performance of the models on the testing dataset is further discussed in Table 4.

Table 4 provides the performance metrics of the developed models for estimating Cd^{2+} absorption by halloysite. The metrics used are MAE, RMSE, and R^2. The models were evaluated on both the training and testing datasets. We can see that the differential evolution multi-layer perceptron (DE-MLP) model has the lowest MAE and RMSE values on both the training and testing datasets, indicating that it has the best performance. However, the R^2 value of the DE-MLP model is lower than the other two models on the testing dataset, indicating that it has a weaker correlation between the predicted and actual values.

In conclusion, the developed models show reasonable performance in predicting the Cd^{2+} absorption efficiency by halloysite on the training dataset. However, their performance on the testing dataset is not as good, indicating that the models may have to overfit the training data. This problem occurred due to the small dataset used. To avoid this problem and achieve better performance on the testing dataset, a larger dataset is required in future works. The DE-MLP model has the best performance on both datasets, but its R^2 value on the testing dataset suggests that it may not be the best model for predicting Cd^{2+} absorption efficiency by halloysite.

Although the obtained results are as good, however, there are some limitations of this study, including:

- The developed models were only tested on one type of clay mineral (halloysite), and their performance on other types of clay minerals may be different.
- The study only considered the Cd^{2+} absorption efficiency, and the models may not perform as well in predicting the absorption efficiency of other heavy metals or pollutants.
- The dataset used for training and testing the models was relatively small, which may limit the generalizability of the results.

8 Conclusion

The present study investigated the ability of three different ANNs models, namely, DE-ANN, PSO-ANN, and SMA-ANN, to predict the efficiency of Cd^{2+} absorption by halloysite. The results of the study show that all three

models can effectively predict the Cd^{2+} absorption efficiency with high accuracy. However, the DE-ANN model exhibited the highest prediction accuracy on the training dataset, while the PSO-ANN model performed the best on the testing dataset.

The performance metrics of the models, as presented in Table 4, demonstrate that the DE-ANN model outperforms the other models in terms of the MAE, RMSE, and R^2 on the training dataset. However, the PSO-ANN model showed better performance on the testing dataset with lower MAE, RMSE, and R^2 values than the other models.

Overall, the study highlights the potential of using ANN models for predicting the Cd^{2+} absorption efficiency by halloysite, and the results suggest that these models can provide accurate and reliable predictions for this application. However, further research is needed to investigate the generalizability of these models to different datasets and conditions.

Based on the obtained results as well as the limitations provided, future works are necessary to enhance the results of this study, as follows:

- The developed models can be further validated using a larger dataset and different types of clay minerals to test their performance and generalizability.
- The study only considered the Cd^{2+} absorption efficiency and future studies can investigate the potential of the developed models for predicting the absorption efficiency of other heavy metals or pollutants.
- Other machine learning algorithms, such as decision trees, support vector machines, extreme gradient boosting machines, extreme learning machines, and other metaheuristic algorithms can be explored to develop more accurate models for predicting the Cd^{2+} absorption efficiency by clay minerals.

Acknowledgments

We gratefully acknowledge the support of the Centre for Excellence in Analysis and Experiment, Hanoi University of Mining and Geology (HUMG), Vietnam, in facilitating the analysis of hallosyte's ability to absorb heavy metals in this study. The authors also extend heartfelt gratitude to Hanoi University of Mining and Geology (Vietnam) and the University of Texas at El Paso (United States) for their invaluable cooperation.

References

[1] M. Balali-Mood, K. Naseri, Z. Tahergorabi, M.R. Khazdair, M. Sadeghi, Toxic mechanisms of five heavy metals: mercury, lead, chromium, cadmium, and arsenic, Front. Pharmacol. 12 (2021).

[2] J. Briffa, E. Sinagra, R. Blundell, Heavy metal pollution in the environment and their toxicological effects on humans, Heliyon 6 (2020) e04691.

[3] M. Adnan, B. Xiao, P. Xiao, P. Zhao, R. Li, S. Bibi, Research progress on heavy metals pollution in the soil of smelting sites in China, Toxics 10 (2022) 231.

[4] K. Soni, M. Amarnath, Heavy metal contamination, in: L.L. Marcelo, S. Sonia (Eds.), Soil Contamination, IntechOpen, Rijeka, 2021. Ch. 1.
[5] M.H. Hegazy, A. Essam, A.Y. Elnaggar, E.E. Hussein, Heavy metal removal from the water of the River Nile using riverbank filtration, Water 13 (2021) 3642.
[6] S. Raja, H.M.N. Cheema, S. Babar, A.A. Khan, G. Murtaza, U. Aslam, Socio-economic background of wastewater irrigation and bioaccumulation of heavy metals in crops and vegetables, Agric. Water Manag. 158 (2015) 26–34.
[7] M.M. Zareh, A.S. El-Sayed, D.M. El-Hady, Biosorption removal of iron from water by *Aspergillus niger*, npj Clean Water 5 (2022) 58.
[8] C. Bai, L. Wang, Z. Zhu, Adsorption of Cr (III) and Pb (II) by graphene oxide/alginate hydrogel membrane: characterization, adsorption kinetics, isotherm and thermodynamics studies, Int. J. Biol. Macromol. 147 (2020) 898–910.
[9] A. Abu-Nada, G. McKay, A. Abdala, Recent advances in applications of hybrid graphene materials for metals removal from wastewater, Nano 10 (2020) 595.
[10] B.H. Bac, H. Nguyen, N.T.T. Thao, V.T. Hanh, L.T. Duyen, N.T. Dung, N.K. Du, N.H. Hiep, Estimating heavy metals absorption efficiency in an aqueous solution using nanotube-type halloysite from weathered pegmatites and a novel Harris hawks optimization-based multiple layers perceptron neural network, Eng. Comput. 38 (2022) 4257–4272.
[11] D. Chauhan, A. Kumar, S.G. Warkar, An efficient adsorbent for the removal of Zn2+ Cd2+ and Hg2+ from the real industrial effluents, Int. J. Environ. Sci. Technol. 19 (2022) 1483–1494.
[12] M.A. Fawzy, H. Darwish, S. Alharthi, M.I. Al-Zaban, A. Noureldeen, S.H.A. Hassan, Process optimization and modeling of Cd2+ biosorption onto the free and immobilized *Turbinaria ornata* using Box–Behnken experimental design, Sci. Rep. 12 (2022) 3256.
[13] W.-L. Jin, X. Ji, X.-L. Hou, S.-Y. Ji, W. Li, X. Yu, X.-W. Liu, L.-N. Zhu, H.-X. Jiang, D.-M. Kong, Porphyrin COF and its mechanical pressing-prepared carbon fiber hybrid membrane for ratiometric detection, removal and enrichment of Cd2+, J. Hazard. Mater. 439 (2022) 129574.
[14] L.M.B. Moungam, K.V. Tchieda, H. Mohamed, N.C. Pecheu, R.C. Kaze, E. Kamseu, A.D. Mvondo-Ze, I.K. Tonle, Efficiency of volcanic ash-based porous geopolymers for the removal of Pb2+, Cd2+ and Hg2+ from aqueous solution, Clean. Mater. 5 (2022) 100106.
[15] K.P. Singh, S. Gupta, P. Ojha, P. Rai, Predicting adsorptive removal of chlorophenol from aqueous solution using artificial intelligence based modeling approaches, Environ. Sci. Pollut. Res. 20 (2013) 2271–2287.
[16] M. Fawzy, M. Nasr, H. Nagy, S. Helmi, Artificial intelligence and regression analysis for Cd(II) ion biosorption from aqueous solution by *Gossypium barbadense* waste, Environ. Sci. Pollut. Res. 25 (2018) 5875–5888.
[17] M. Dolatabadi, M. Mehrabpour, M. Esfandyari, H. Alidadi, M. Davoudi, Modeling of simultaneous adsorption of dye and metal ion by sawdust from aqueous solution using of ANN and ANFIS, Chemom. Intell. Lab. Syst. 181 (2018) 72–78.
[18] M. Fan, J. Hu, R. Cao, W. Ruan, X. Wei, A review on experimental design for pollutants removal in water treatment with the aid of artificial intelligence, Chemosphere 200 (2018) 330–343.
[19] H. Lu, H. Li, T. Liu, Y. Fan, Y. Yuan, M. Xie, X. Qian, Simulating heavy metal concentrations in an aquatic environment using artificial intelligence models and physicochemical indexes, Sci. Total Environ. 694 (2019) 133591.
[20] E. Rahnama, O. Bazrafshan, G. Asadollahfardi, Application of data-driven methods to predict the sodium adsorption rate (SAR) in different climates in Iran, Arab. J. Geosci. 13 (2020) 1160.

[21] A. El Hanandeh, Z. Mahdi, M.S. Imtiaz, Modelling of the adsorption of Pb, cu and Ni ions from single and multi-component aqueous solutions by date seed derived biochar: comparison of six machine learning approaches, Environ. Res. 192 (2021) 110338.

[22] J.A. Rodríguez-Romero, D.I. Mendoza-Castillo, H.E. Reynel-Ávila, D.A. de Haro-Del Rio, L. M. González-Rodríguez, A. Bonilla-Petriciolet, C.J. Duran-Valle, K.I. Camacho-Aguilar, Preparation of a new adsorbent for the removal of arsenic and its simulation with artificial neural network-based adsorption models, J. Environ. Chem. Eng. 8 (2020) 103928.

[23] A. Das, N. Bar, S.K. Das, Pb(II) adsorption from aqueous solution by nutshells, green adsorbent: adsorption studies, regeneration studies, scale-up design, its effect on biological indicator and MLR modeling, J. Colloid Interface Sci. 580 (2020) 245–255.

[24] M. Fawzy, M. Nasr, S. Adel, H. Nagy, S. Helmi, Environmental approach and artificial intelligence for Ni(II) and Cd(II) biosorption from aqueous solution using *Typha domingensis* biomass, Ecol. Eng. 95 (2016) 743–752.

[25] L.T. Popoola, Nano-magnetic walnut shell-rice husk for Cd(II) sorption: design and optimization using artificial intelligence and design expert, Heliyon 5 (2019) e02381.

[26] J. Qi, Y. Hou, J. Hu, W. Ruan, Y. Xiang, X. Wei, Decontamination of methylene blue from simulated wastewater by the mesoporous rGO/Fe/Co nanohybrids: artificial intelligence modeling and optimization, Mater. Today Commun. 24 (2020) 100709.

[27] E. Salehi, J. Abdi, M.H. Aliei, Assessment of cu(II) adsorption from water on modified membrane adsorbents using LS-SVM intelligent approach, J. Saudi Chem. Soc. 20 (2016) 213–219.

[28] T. Shojaeimehr, F. Rahimpour, M.A. Khadivi, M. Sadeghi, A modeling study by response surface methodology (RSM) and artificial neural network (ANN) on Cu2+ adsorption optimization using light expended clay aggregate (LECA), J. Ind. Eng. Chem. 20 (2014) 870–880.

[29] P.R. Souza, G.L. Dotto, N.P.G. Salau, Artificial neural network (ANN) and adaptive neuro-fuzzy interference system (ANFIS) modelling for nickel adsorption onto agro-wastes and commercial activated carbon, J. Environ. Chem. Eng. 6 (2018) 7152–7160.

[30] M. Zafar, N. Van Vinh, S.K. Behera, H.-S. Park, Ethanol mediated As(III) adsorption onto Zn-loaded pinecone biochar: experimental investigation, modeling, and optimization using hybrid artificial neural network-genetic algorithm approach, J. Environ. Sci. 54 (2017) 114–125.

[31] L. Zhao, T. Dai, Z. Qiao, P. Sun, J. Hao, Y. Yang, Application of artificial intelligence to wastewater treatment: a bibliometric analysis and systematic review of technology, economy, management, and wastewater reuse, Process Saf. Environ. Prot. 133 (2020) 169–182.

[32] S. Agatonovic-Kustrin, R. Beresford, Basic concepts of artificial neural network (ANN) modeling and its application in pharmaceutical research, J. Pharm. Biomed. Anal. 22 (2000) 717–727.

[33] A. Shrestha, A. Mahmood, Review of deep learning algorithms and architectures, IEEE Access 7 (2019) 53040–53065.

[34] Z. Zhao, S. Xu, B.H. Kang, M.M.J. Kabir, Y. Liu, R. Wasinger, Investigation and improvement of multi-layer perceptron neural networks for credit scoring, Expert Syst. Appl. 42 (2015) 3508–3516.

[35] T.G. Tan, J. Teo, P. Anthony, A comparative investigation of non-linear activation functions in neural controllers for search-based game AI engineering, Artif. Intell. Rev. 41 (2014) 1–25.

[36] S. Li, H. Chen, M. Wang, A.A. Heidari, S. Mirjalili, Slime mould algorithm: a new method for stochastic optimization, Futur. Gener. Comput. Syst. 111 (2020) 300–323.

[37] H. Gao, G. Liang, H. Chen, Multi-population enhanced slime mould algorithm and with application to postgraduate employment stability prediction, Electronics 11 (2022) 209.

[38] D. Wang, D. Tan, L. Liu, Particle swarm optimization algorithm: an overview, Soft. Comput. 22 (2018) 387–408.

[39] S. Rana, S. Jasola, R. Kumar, A review on particle swarm optimization algorithms and their applications to data clustering, Artif. Intell. Rev. 35 (2011) 211–222.
[40] X. Zhang, H. Nguyen, X.-N. Bui, H. Anh Le, T. Nguyen-Thoi, H. Moayedi, V. Mahesh, Evaluating and predicting the stability of roadways in tunnelling and underground space using artificial neural network-based particle swarm optimization, Tunn. Undergr. Space Technol. 103 (2020) 103517.
[41] X.-N. Bui, P. Jaroonpattanapong, H. Nguyen, Q.-H. Tran, N.Q. Long, A novel hybrid model for predicting blast-induced ground vibration based on k-nearest neighbors and particle swarm optimization, Sci. Rep. 9 (2019) 1–14.
[42] H. Nguyen, H.-B. Bui, X.-N. Bui, Rapid determination of gross calorific value of coal using artificial neural network and particle swarm optimization, Nat. Resour. Res. 30 (2021) 621–638.
[43] M. Georgioudakis, V. Plevris, A comparative study of differential evolution variants in constrained structural optimization, Front. Built Environ. 6 (2020) 102.
[44] S. Prabha, R. Yadav, Differential evolution with biological-based mutation operator, Eng. Sci. Technol. Int. J. 23 (2020) 253–263.
[45] S. Li, W. Gong, L. Wang, X. Yan, C. Hu, Optimal power flow by means of improved adaptive differential evolution, Energy 198 (2020) 117314.
[46] K. Price, R.M. Storn, J.A. Lampinen, Differential Evolution: A Practical Approach to Global Optimization, Springer Science & Business Media, 2006.
[47] S.M. Karazi, M. Moradi, K.Y. Benyounis, Statistical and numerical approaches for modeling and optimizing laser micromachining process-review, in: Reference Module in Materials Science and Materials Engineering, Elsevier, 2019.
[48] B.K. Lavine, T.R. Blank, 3.18 – Feed-forward neural networks, in: S.D. Brown, R. Tauler, B. Walczak (Eds.), Comprehensive Chemometrics, Elsevier, Oxford, 2009, pp. 571–586.
[49] B.G.M. Vandeginste, D.L. Massart, L.M.C. Buydens, S. De Jong, P.J. Lewi, J. Smeyers-Verbeke, Chapter 44: Artificial neural networks, in: B.G.M. Vandeginste, D.L. Massart, L. M.C. Buydens, S. De Jong, P.J. Lewi, J. Smeyers-Verbeke (Eds.), Data Handling in Science and Technology, Elsevier, 1998, pp. 649–699.